

Supplemental Information

Multimodal Electrochemistry Coupled Microcalorimetric and X-ray Probing of the Capacity Fade Mechanisms of Nickel Rich NMC – Progress and Outlook

Calvin D. Quilty^{‡ab}, Patrick J. West^{‡bc}, Wenzao Li^{‡ab}, Mikaela R. Dunkin^{bc}, Garrett P.

Wheeler^b, Steven Ehrlich^d, Lu Ma^d, Cherno Jaye^e, Daniel A. Fischer^e, Esther S.

Takeuchi^{abcf}, Kenneth J. Takeuchi^{abcf}, David C. Bock^{bf*}, Amy C. Marschilok^{abcf*}

- a. Department of Chemistry, State University of New York at Stony Brook, Stony Brook, New York 11794, United States.
- b. Institute for Electrochemically Stored Energy, State University of New York at Stony Brook, Stony Brook, New York 11794, United States.
- c. Department of Materials Science and Chemical Engineering, State University of New York at Stony Brook, Stony Brook, New York 11794, United States.
- d. National Synchrotron Light Source II, Brookhaven National Laboratory, Upton, New York 11973, United States.
- e. Material Measurement Laboratory, National Institute of Standards and Technology, Gaithersburg, Maryland 20899
- f. Interdisciplinary Science Department, Brookhaven National Laboratory, Upton, New York 11973, United States.

‡Denotes equivalent contributions. Mikaela Dunkin 0000-0003-0328-0020; Garret Wheeler 0000-0003-3097-4183; Cherno Jaye 0000-0001-6158-6373; Daniel A. Fischer 0000-0002-3072-6000; Esther Takeuchi 0000-0001-8518-1047; Kenneth Takeuchi 0000-0001-8129-444X; David Bock 0000-0002-2387-7791; Amy Marschilok 0000-0001-9174-0474

*corresponding authors: (DCB) dbock@bnl.gov, (ACM) amy.marschilok@stonybrook.edu

Experimental

Cell Construction

90% NMC811 (Targray) was combined with 5% Super P conductive carbon and 5% polyvinylidene fluoride binder and tape-cast on to carbon-coated aluminum foil. The active mass loading was 7 mg/cm². The NMC811 composite cathodes were integrated

into CR2032 coin cells and custom-built pouch cells, optimized for beamline X-ray absorption and/or lab-based X-ray diffraction measurements. In all cases, lithium foil was used as the counter/reference electrode, 1 M LiPF₆ in 3:7 ethylene carbonate: dimethyl carbonate was the electrolyte, and Tonen polypropylene separators were employed.

Electrochemical Testing

Galvanostatic cycling was performed on a Maccor battery cycler as well as a BioLogic VSP multichannel potentiostat. Electrochemical impedance spectroscopy (EIS) was performed in the discharged state on the BioLogic VSP multichannel potentiostat. Coin cells underwent three formation cycles at C/10 (1C=190 mA/g) at 3.0 V to either 4.3 or 4.7 V, following the formation cycling the cells were cycled 100 times at C/2 with the same potential windows. EIS was collected at the discharged state before and after cycling from 100 kHz-10 mHz, $V_a=10$ mV, and $p_w=0.1$. Pouch cells underwent two formation cycles at C/10 at either 3-4.3 or 3-4.7 V, following the formation cycling the cells were cycled 100 times at 1C with the same potential windows.

***Operando* isothermal microcalorimetry**

A TAM IV (TA Instruments) isothermal microcalorimeter was used to perform the IMC experiment. Coin-type cells were placed in holding ampules and submerged in an oil bath in which the temperature was rigorously controlled at 30 °C. Coin cells were simultaneously connected to a BioLogic VSP potentiostat for electrochemical cycling. Prior to the IMC test, NMC622/Li cells were pre-cycled in 3-4.1 V for 3 cycles and in either 3-4.3 V or 3-4.7 V for 2 additional cycles. During the IMC test, cells were cycled with two potential limits (4.3 V or 4.7 V) at four C-rates (C/10, C/5, C/2, 1C). Following each charge and discharge step, the cell potential was held until the response current dropped to a

C/10 equivalence. A 12-hour rest in open-circuit condition was introduced after all charge and discharge steps to realize the thermal equilibrium.

Operando X-ray Diffraction

Cathodes (either fresh or previously cycled in coin cells) were integrated into NMC811/Li pouch cells designed for lab-based XRD measurements. The coin cells were decrimped in an argon glovebox and the cathodes were transferred to a humidity controlled dry room (~100 ppm water vapor) where the pouch cells were assembled. The pouch cells were cycled once at C/10 from either 3-4.3 or 4.7 V while XRD patterns were collected. XRD patterns were collected on a Rigaku SmartLab with a Cu K α X-ray source and a D/Tex Ultra 1D detector. One pattern was collected every 27 minutes. Patterns were fit with the GSAS-II software package.¹ The patterns were fit with one $R\bar{3}m$ NMC811 structural model. The material was designated H1, H2, or H3 at a given point of lithiation based on the changes in the unit cell, where the *a* axis contraction and *c* axis expansion was the H1 to H2 transition and the subsequent *c* axis contraction was the H2 to H3 transition.

Scanning Electron Microscopy

Scanning electron microscopy (SEM) images were collected with a JEOL JSM-7600F microscope at an accelerating voltage of 5 kV. Images were collected on a pristine cathode and on previously cycled cathodes. The previously cycled cathodes were cycled 100 times in a coin cell vs. Li/Li⁺ at a rate of C/2 and a potential window of 3-4.3 or 3-4.7 V. The cells were deconstructed in the discharged state and the cathodes were rinsed with dimethyl carbonate and dried *in vacuo*.

Operando X-ray Absorption Spectroscopy

XAS measurements were collected at beamline 7-BM at the National Synchrotron Light Source II at Brookhaven National Laboratory. Pouch cells (both fresh and previously cycled cells) that were designed for beamline X-ray characterization were cycled once at either 3-4.3 or 3-4.7 V at C/5. XAS measurements were collected as the cells cycled at the nickel, manganese, and cobalt K-edges, 8333, 6539, and 7709 eV respectively. The data was normalized, merged, and calibrated in Athena.^{2, 3} Linear combination fitting (LCF) was performed in Athena with a fit range of -30 to 30 eV in the $\mu(E)$ fitting space. Manganese spectra were fit to Mn_2O_3 and MnO_2 standards while cobalt spectra were fit to $LiCoO_2$ and $Li_{0.389}CoO_2$ standards. These LCF results were used to determine the oxidation state of nickel based on electroneutrality.

EXAFS fitting was performed using a structural model based on $LiNiO_2$ structure with a $R\bar{3}m$ space group, with two scattering paths were used to model Ni-O and Ni-M distances. The coordination number and amplitude reduction factor were held constant allowing for the Debye-Waller disorder factors to be determined. A single path was used to model Ni-O bonds, consistent with previous EXAFS studies of NMC materials with lower Ni content.⁴⁻⁸ Peak broadening associated with multiple bond lengths from Jahn Teller distortion in Ni^{3+} were tracked using the Debye Waller factor for the Ni-O path, σ_{Ni-O}^2 . The value of σ_{Ni-O}^2 was found to be directly correlated with the population of Ni^{3+} determined from the XANES LCF analysis, with maximum disorder observed in the lithiated state. These results are consistent with prior reports which also showed an increase in Debye-Waller factor with increased lithiation level.^{4, 5}

Soft X-ray Absorption Spectroscopy

Cathodes were harvested from NMC811 coin cells that had either experienced formation cycling only, or 50 cycles as described above. The cathodes were removed from the coin cell, rinsed with DMC, and stored in an argon glovebox prior to analysis. sXAS measurements were collected at beamline 7-ID-1 at the National Synchrotron Light Source II at Brookhaven National Laboratory. The Ni, Mn, and Co L-edges and O K-edge were measured between 515 – 900 eV under vacuum. NiO and LiNiO₂ (Sigma-Aldrich; purity $\geq 98\%$) standards were prepared in 95 wt% BN pellets and sealed between Kapton tape. The MnO, Mn₂O₃, MnO₂, Mn₃O₄, LiCoO₂, and Li_{0.389}CoO₂ were prepared similarly. Data processing was done in Athena and Origin.

Disclaimer: Identification of commercial equipment, instruments, or materials in this paper is not intended to imply recommendation or endorsement by the National Institute of Standards and Technology, nor is it intended to imply that the materials or equipment identified are necessarily the best available for the purpose.

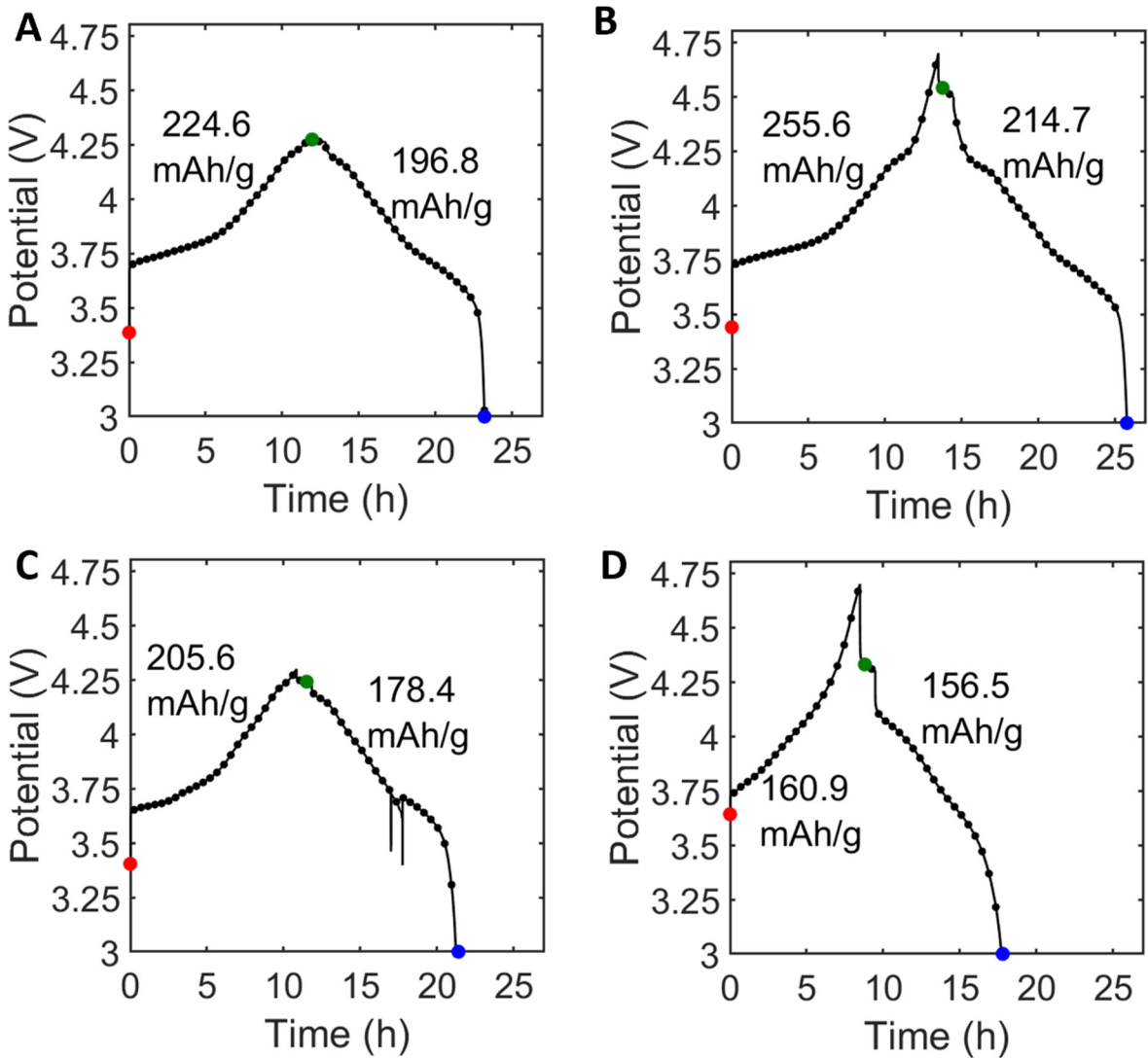


Figure S1. Galvanostatic (dis)charge curves of *operando* XRD NMC811/Li cells. (A) (3 to 4.3) V fresh, (B) (3 to 4.7) V fresh, (C) (3 to 4.3) V cycled, and (D) (3 to 4.7) V cycled. The points represent XRD scans. Red, green, and blue represent scans taken in the pristine, charged, and discharged state respectively.

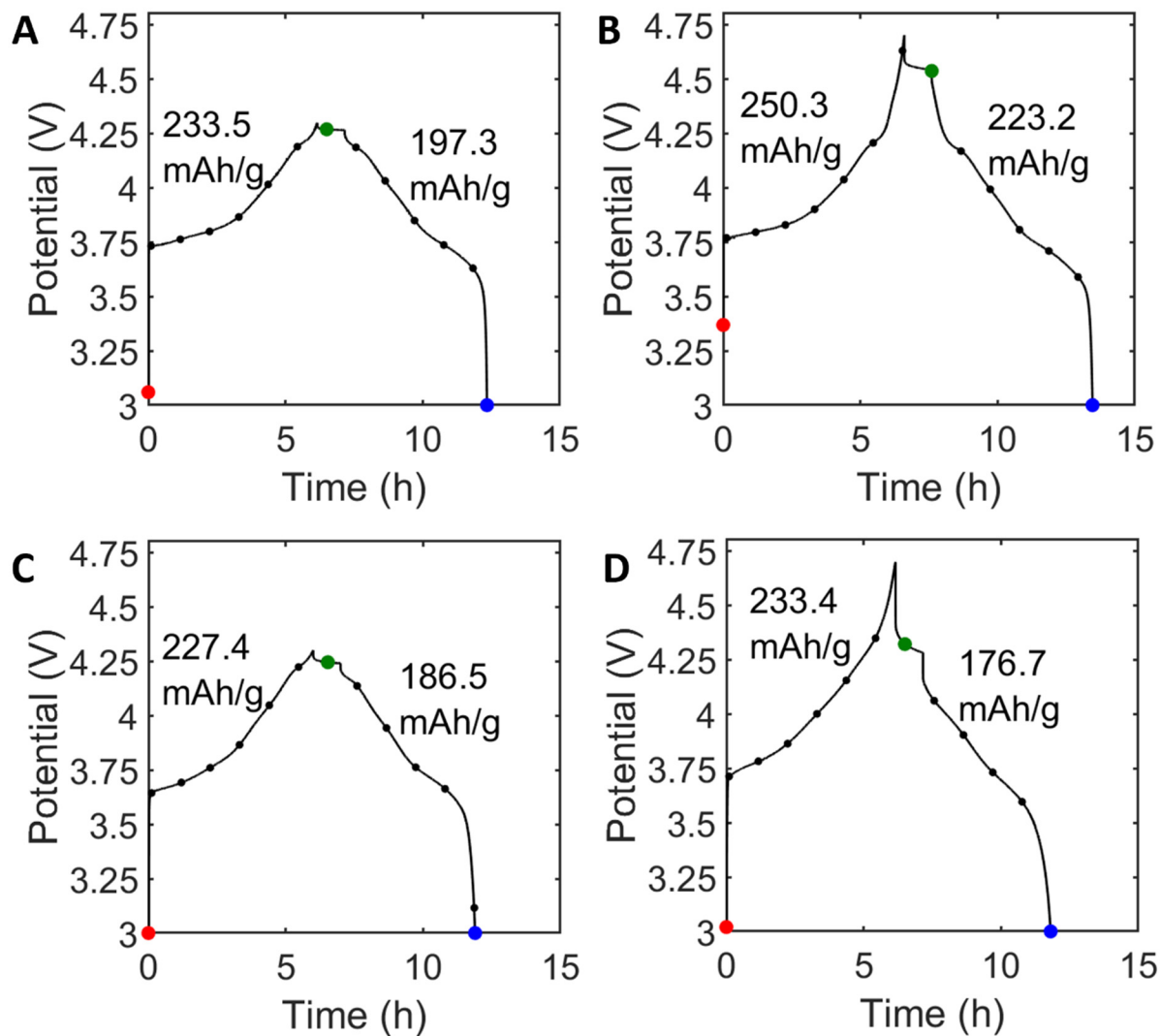


Figure S2. Galvanostatic (dis)charge curves of *operando* XAS NMC811/Li cells. (A) (3 to 4.3) V fresh, (B) (3 to 4.7) V fresh, (C) (3 to 4.3) V cycled, and (D) (3 to 4.7) V cycled. The points represent XAS scans. Red, green, and blue represent scans taken in the pristine, charged, and discharged state respectively.

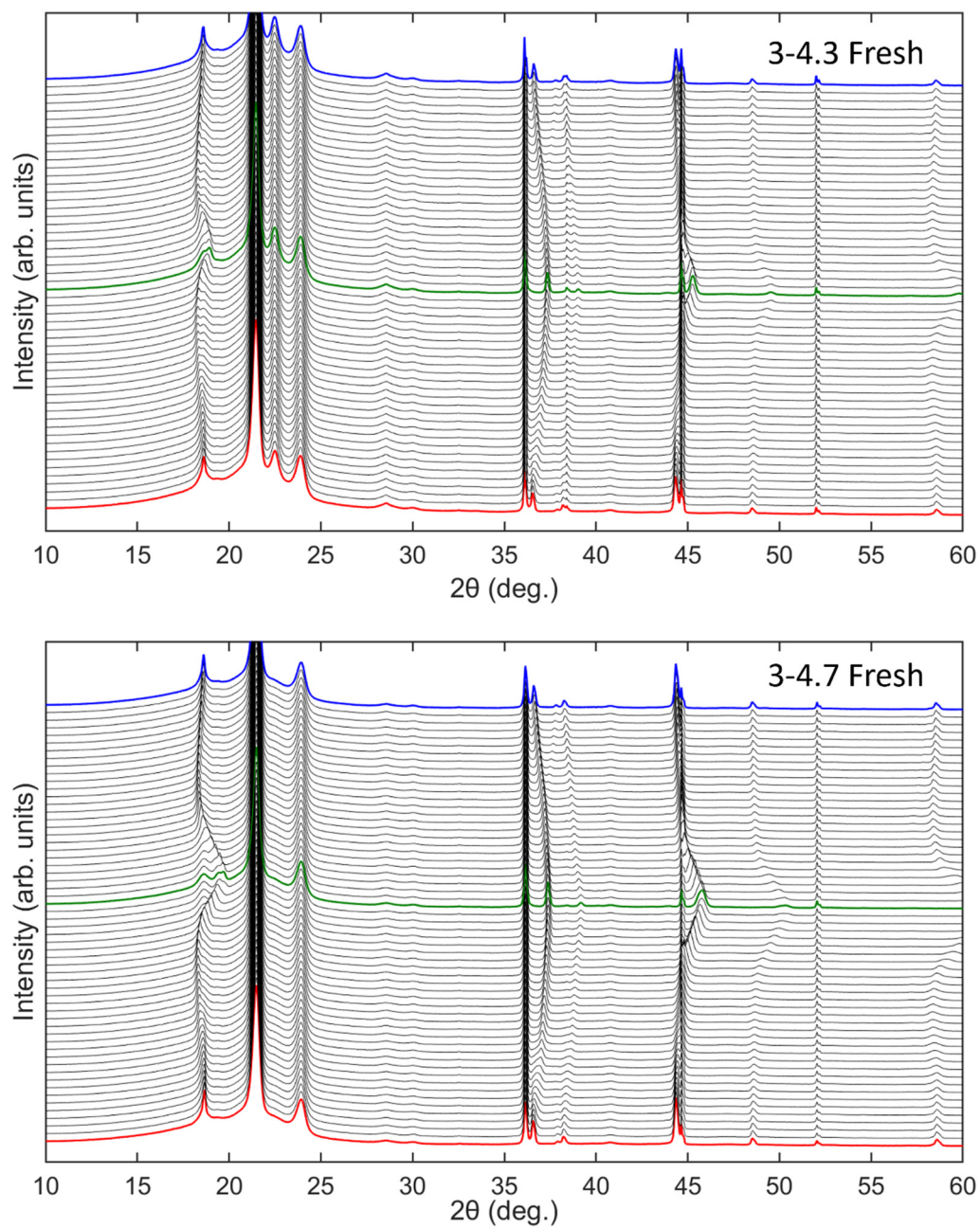


Figure S3. *Operando* XRD patterns collected on 3-4.3 fresh and 3-4.7 V fresh cells. Pristine, charged, and discharged are marked in red, green, and blue respectively.

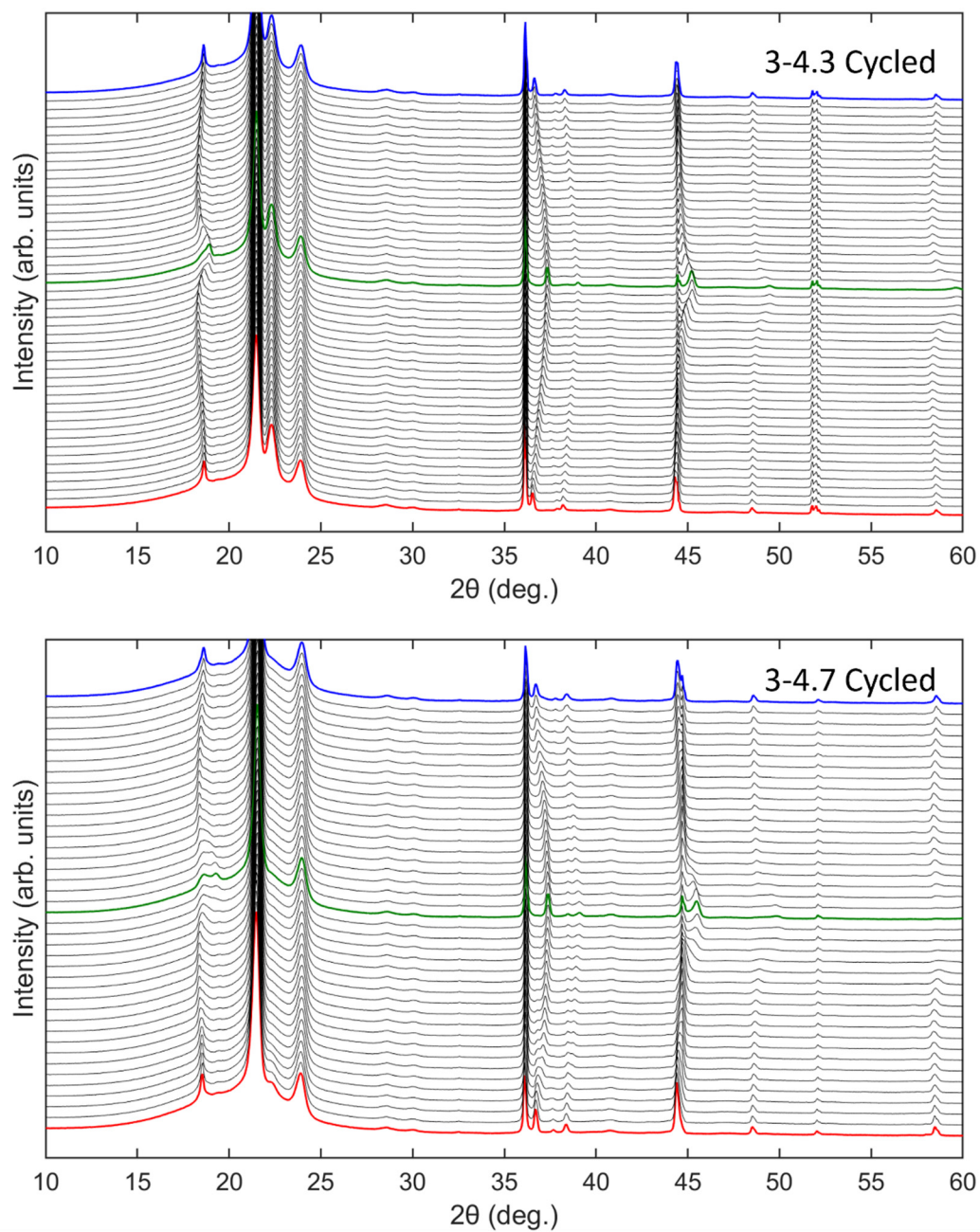


Figure S4. *Operando* XRD patterns collected on 3-4.3 cycled and 3-4.7 V cycled cells. Pristine, charged, and discharged are marked in red, green, and blue respectively.

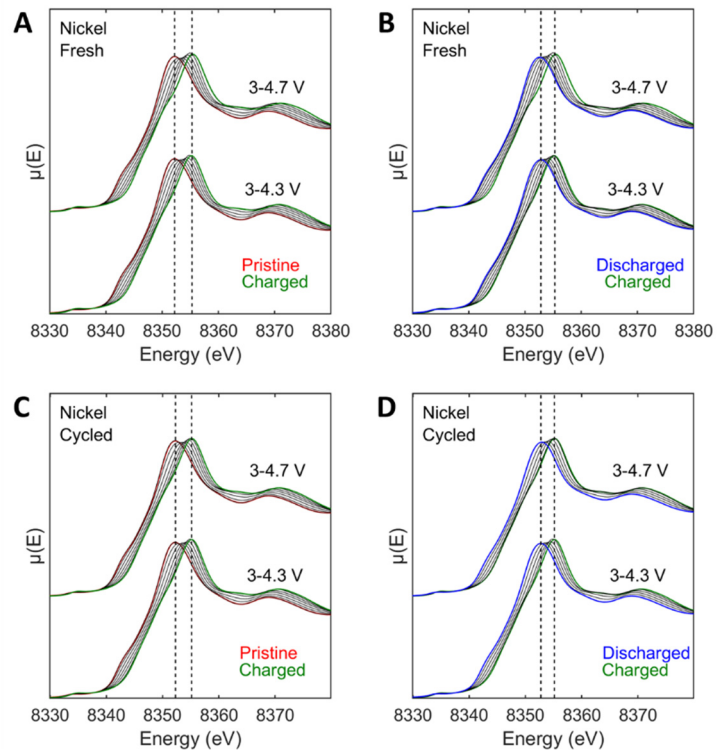


Figure S5. XANES of Ni edge for NMC811/Li pouch cells.

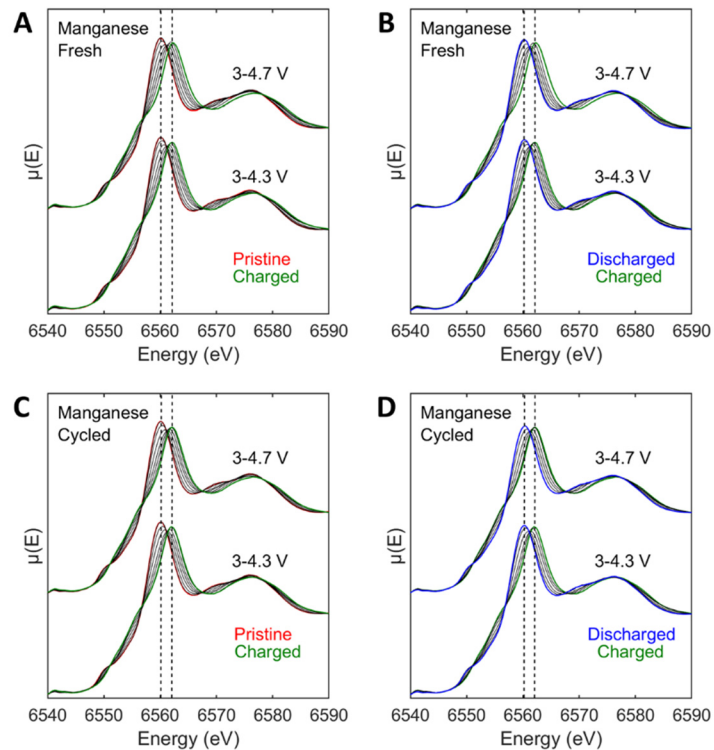


Figure S6. XANES of Mn edge for NMC811/Li pouch cells.

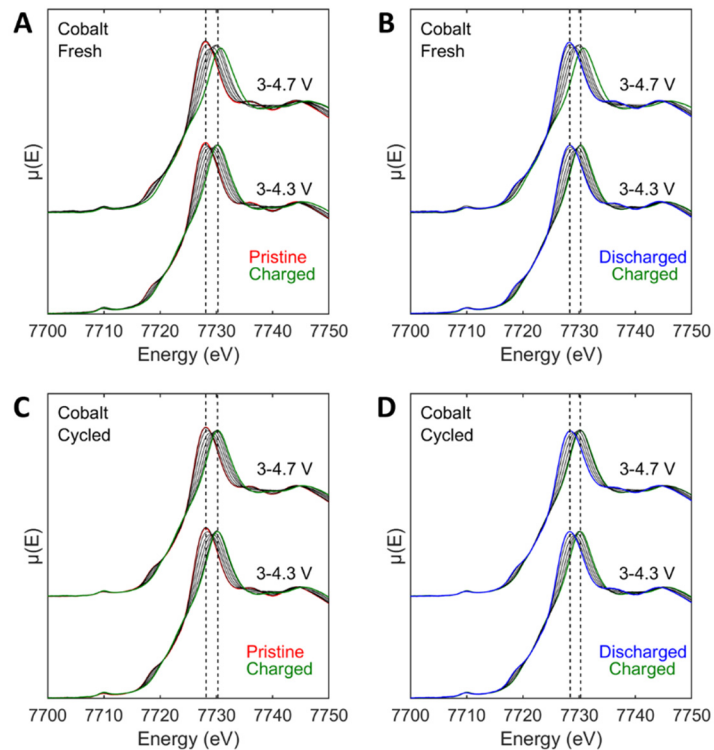


Figure S7. XANES of Co edge for NMC811/Li pouch cells.

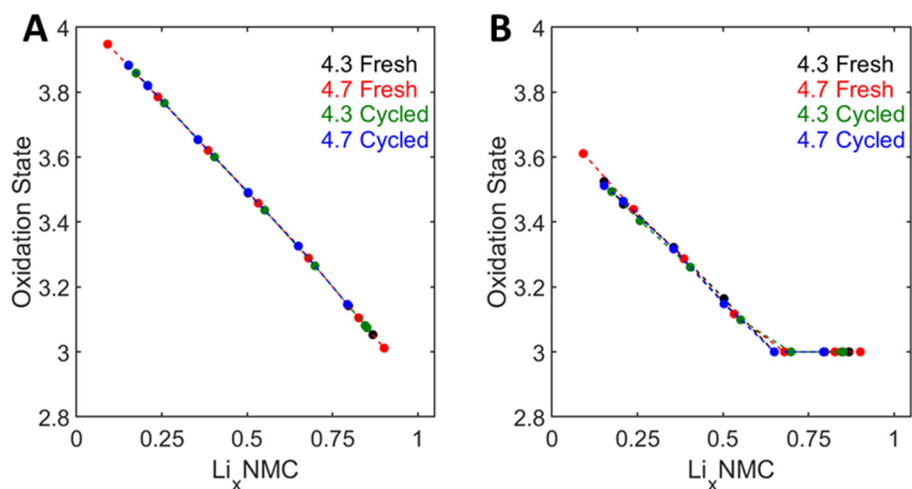


Figure S8. Oxidation state of nickel and cobalt as determined by linear combination fitting of XANES spectra collected on discharging cells. (A) Oxidation states of nickel and (B) cobalt.

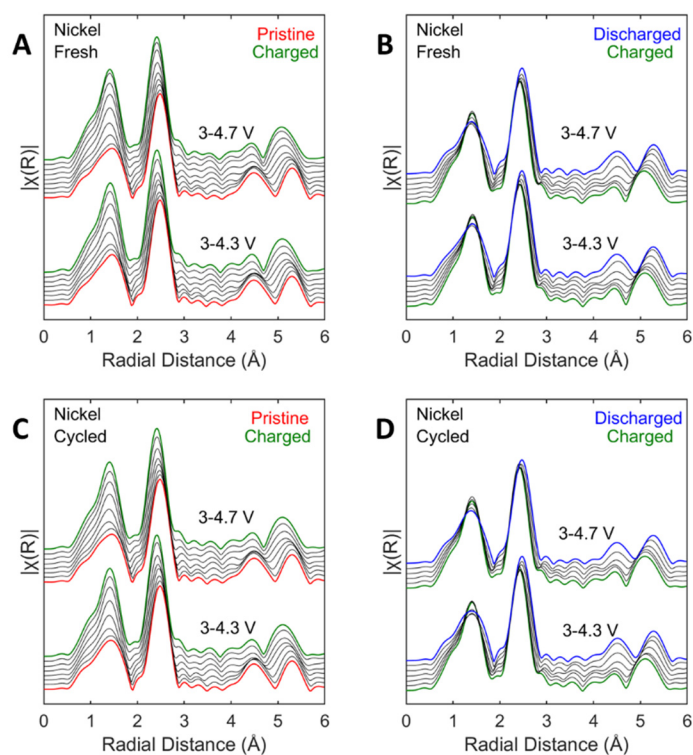


Figure S9. EXAFS of Ni edge for NMC811/Li pouch cells.

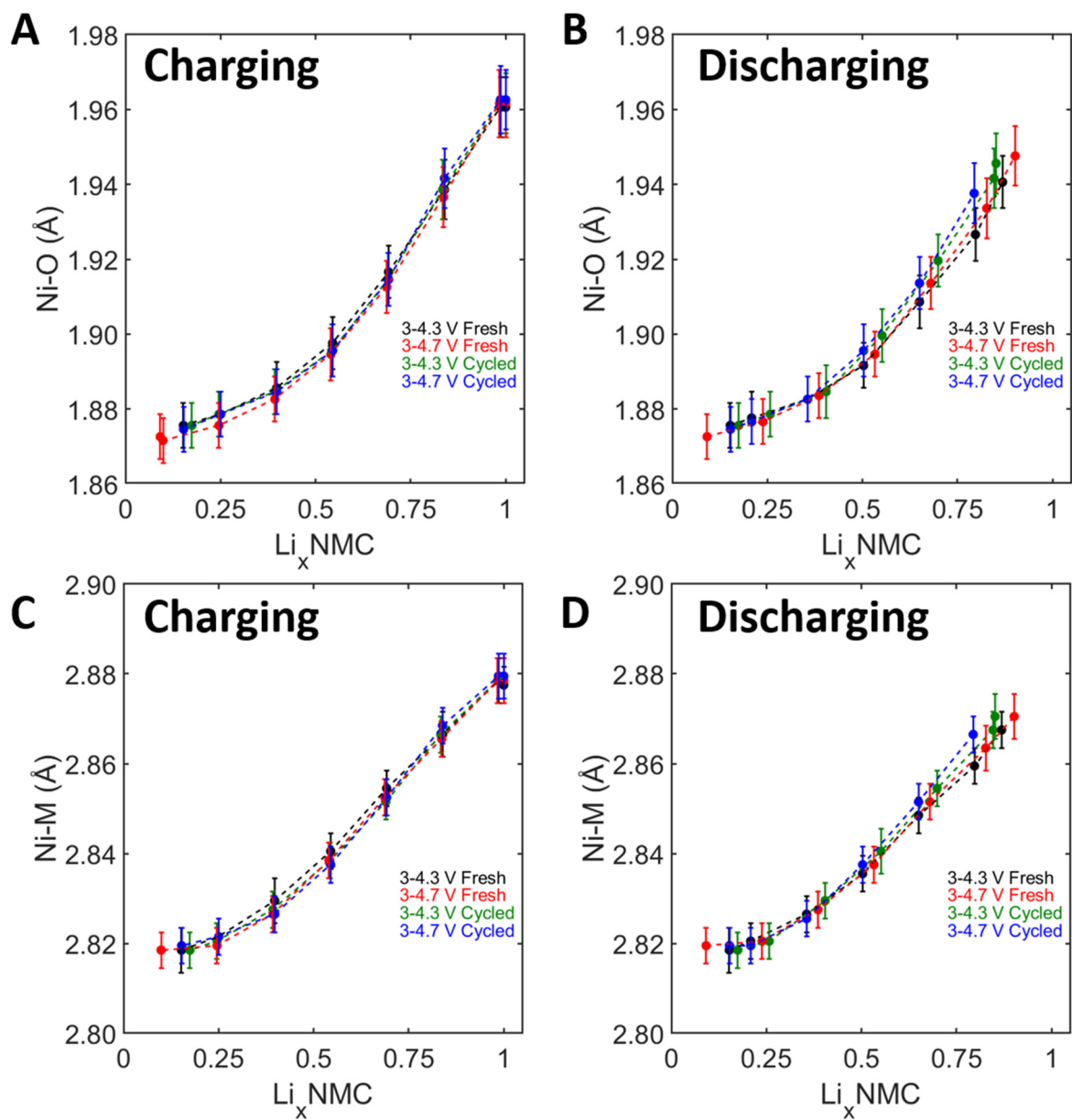


Figure S10. Bond distances of Ni-O and Ni-M as determined by EXAFS. (A) and (B) Bond distances of Ni-O during charge and discharge. (C) and (D) Bond distances of Ni-M during charge and discharge.

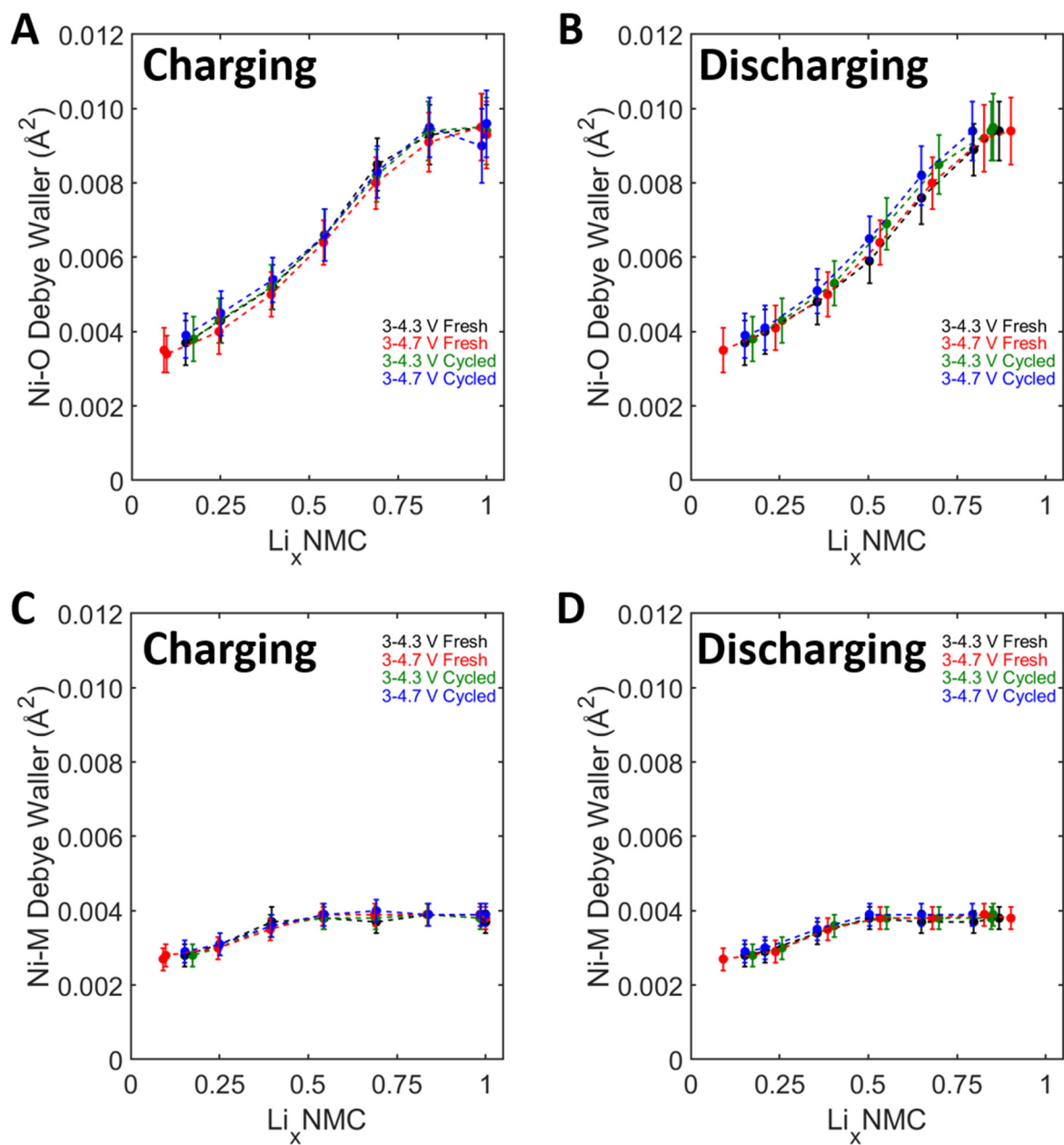


Figure S11. Debye-Waller parameters of Ni-O and Ni-M as determined by EXAFS. (A) and (B) Parameters of Ni-O during charge and discharge. (C) and (D) Parameters of Ni-M during charge and discharge.

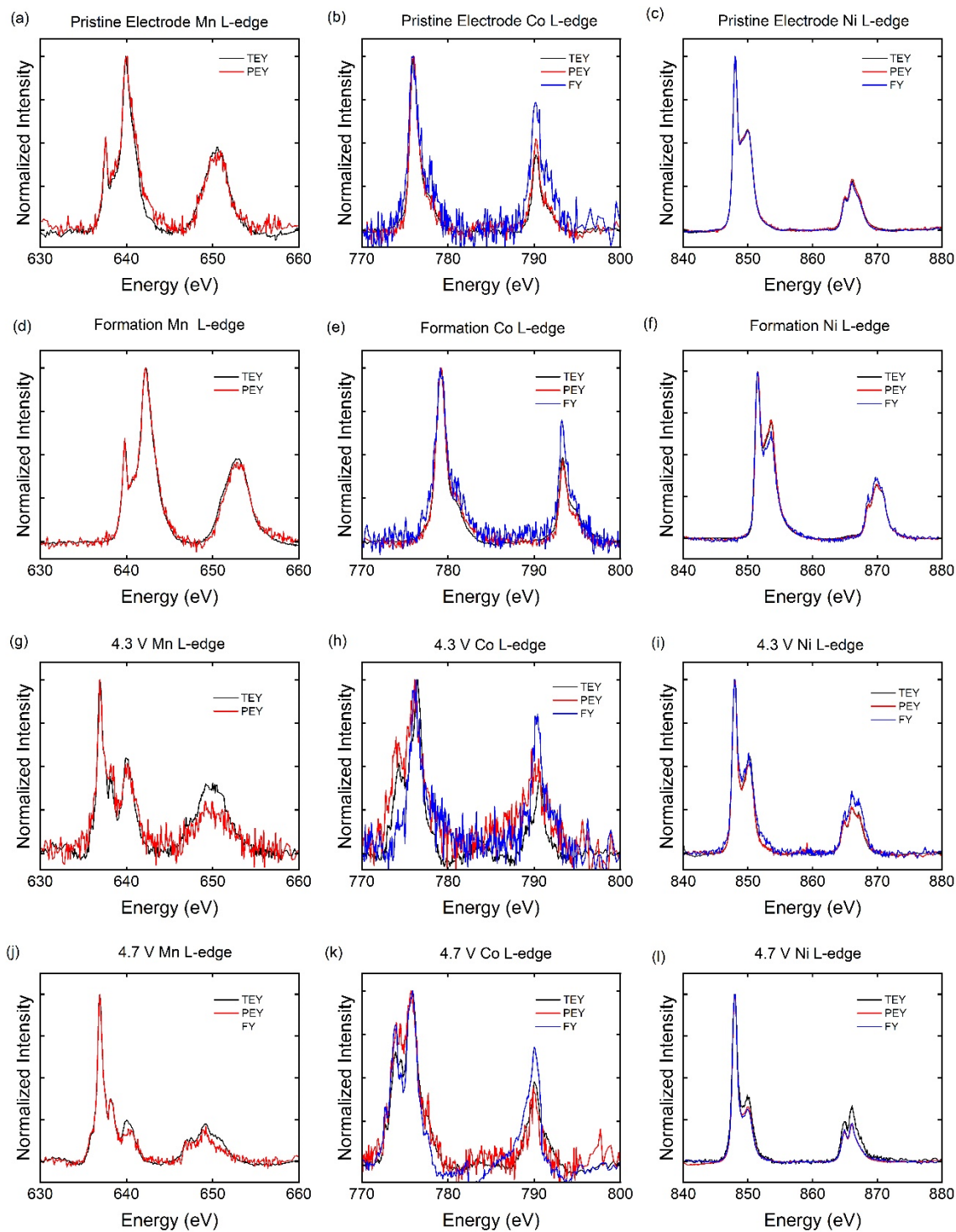


Figure S12. Soft XAS spectra for the Ni, Mn, and Co L-edges for a pristine electrode (a,b,c), an electrode formation cycled (d,e,f), cycled 50 times to 4.3 V (g,h,i), and to 4.7 V (j,k,l).

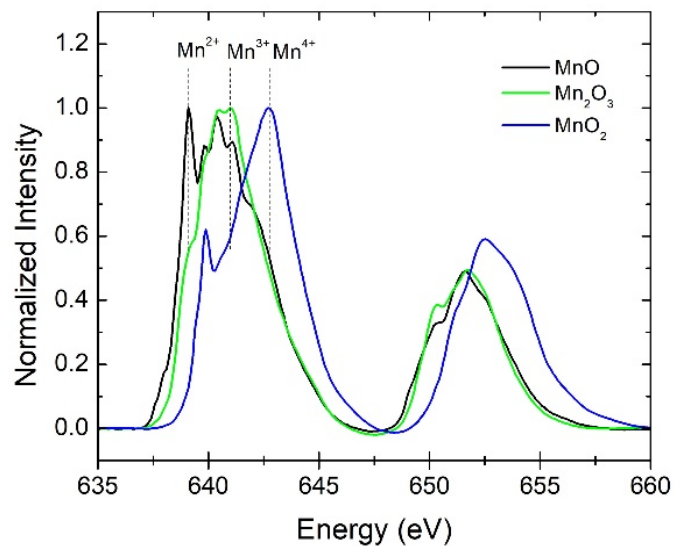


Figure S13. Mn L-edge of various manganese oxide polymorphs.

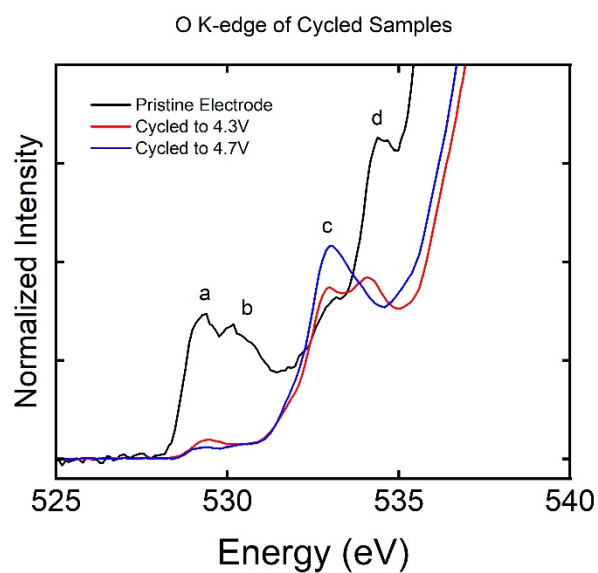


Figure S14. The O K-edge pre-edge region of pristine and cycled NMC811 electrodes.

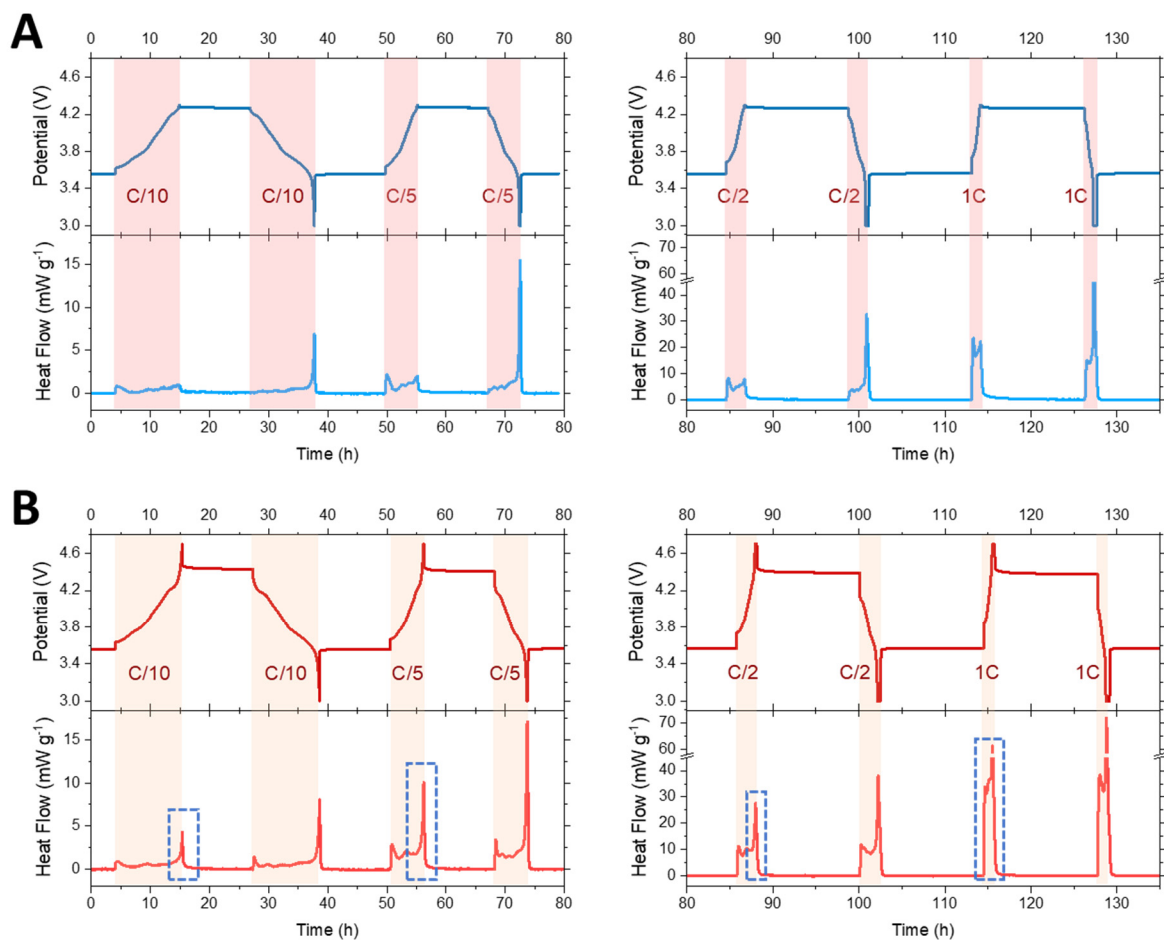


Figure S15. Operando isothermal microcalorimetry of NMC811/Li cells. (A) (3 to 4.3) V at four C-rates of C/10, C/5, C/2, and 1C. (B) (3 to 4.7) V at four C-rates. The heat flow spike (highlighted with blue boxes) occurred at a high state-of-charge when the voltage was above 4.3 V.

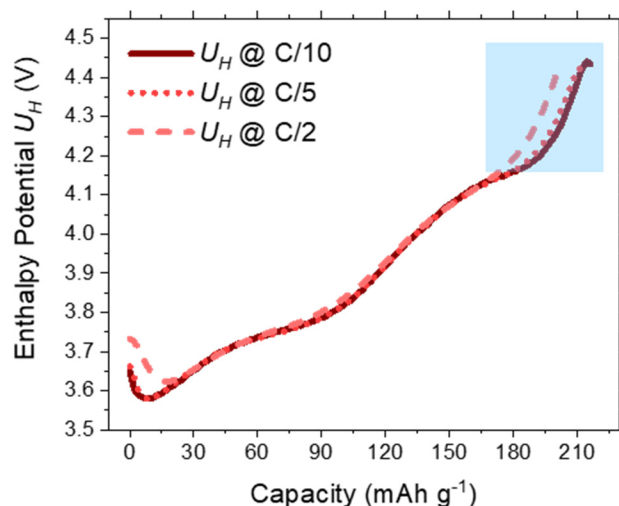


Figure S16. The enthalpy potential plots determined from NMC811 cells charged to 4.7 V at C-rates of C/10, C/5, and C/2. The U_H curves show discrepancies with each other in the high-voltage area (highlighted in blue), which indicates local thermodynamic irreversibility at high voltage.

References

1. Toby, B. H.; Von Dreele, R. B., GSAS-II: the genesis of a modern open-source all purpose crystallography software package. *J. Appl. Crystallogr.* **2013**, *46* (2), 544-549.
2. Newville, M., IFEFFIT: interactive XAFS analysis and FEFF fitting. *J. Synchrotron Radiat.* **2001**, *8* (2), 322-324.
3. Ravel, B.; Newville, M., ATHENA, ARTEMIS, HEPHAESTUS: data analysis for X-ray absorption spectroscopy using IFEFFIT. *J. Synchrotron Radiat.* **2005**, *12* (4), 537-541.
4. Chen, C.-H.; Pan, C.-J.; Su, W.-N.; Rick, J.; Wang, C.-J.; Venkateswarlu, M.; Lee, J.-F.; Hwang, B.-J., Operando X-ray diffraction and X-ray absorption studies of the structural transformation upon cycling excess Li layered oxide $\text{Li}[\text{Li}_{1/18}\text{Co}_{1/6}\text{Ni}_{1/3}\text{Mn}_{4/9}]\text{O}_2$ in Li ion batteries. *Journal of Materials Chemistry A* **2015**, *3* (16), 8613-8626.
5. Tsai, Y. W.; Hwang, B. J.; Ceder, G.; Sheu, H. S.; Liu, D. G.; Lee, J. F., In-Situ X-ray Absorption Spectroscopic Study on Variation of Electronic Transitions and Local Structure of $\text{LiNi}_{1/3}\text{Co}_{1/3}\text{Mn}_{1/3}\text{O}_2$ Cathode Material during Electrochemical Cycling. *Chemistry of Materials* **2005**, *17* (12), 3191-3199.

6. Liao, P.-Y.; Duh, J.-G.; Lee, J.-F.; Sheu, H.-S., Structural investigation of $\text{Li}_{1-x}\text{Ni}_{0.5}\text{Co}_{0.25}\text{Mn}_{0.25}\text{O}_2$ by in situ XAS and XRD measurements. *Electrochimica Acta* **2007**, 53 (4), 1850-1857.
7. Deb, A.; Bergmann, U.; Cramer, S. P.; Cairns, E. J., In Situ X-Ray Absorption Spectroscopic Study of $\text{Li}_{1.05}\text{Ni}_{0.35}\text{Co}_{0.25}\text{Mn}_{0.4}\text{O}_2$ Cathode Material Coated with LiCoO_2 . *Journal of The Electrochemical Society* **2007**, 154 (6), A534.
8. Deb, A.; Bergmann, U.; Cramer, S. P.; Cairns, E. J., In situ x-ray absorption spectroscopic study of the $\text{Li}[\text{Ni}_{1/3}\text{Co}_{1/3}\text{Mn}_{1/3}]\text{O}_2$ cathode material. *Journal of Applied Physics* **2005**, 97 (11), 113523.